THE JOURNAL OF BIOLOGICAL CHEMISTRY
Vol. 279, No. 4, Issue of January 23, pp. 2817–2824, 2004

Printed in U.S.A.

Molecular Basis for Atovaquone Resistance in *Pneumocystis jirovecii* Modeled in the Cytochrome bc_1 Complex of *Saccharomyces cerevisiae**

Received for publication, September 8, 2003, and in revised form, October 20, 2003
Published, JBC Papers in Press, October 23, 2003, DOI 10.1074/jbc.M309984200

Jacques J. Kessl‡, Philip Hill§, Benjamin B. Lange‡, Steven R. Meshnick¶, Brigitte Meunier§, and Bernard L. Trumpower‡‖

From the ‡Department of Biochemistry, Dartmouth Medical School, Hanover, New Hampshire 03755, §Wolfson Institute for Biomedical Research, University College London, London WCIE 6BT, United Kingdom, and ¶Department of Microbiology and Immunology, University of North Carolina, Chapel Hill, North Carolina 27599

Atovaquone is a substituted hydroxynaphthoquinone that is widely used to prevent and clear *Plasmodium falciparum* malaria and *Pneumocystis jirovecii* pneumonia. Atovaquone inhibits respiration in target organisms by specifically binding to the ubiquinol oxidation site at center P of the cytochrome bc_1 complex. The failure of atovaquone treatment and mortality of patients with malaria and *P. jirovecii* pneumonia has been linked to the appearance of mutations in the cytochrome *b* gene. To better understand the molecular basis of atovaquone resistance, we have introduced seven of the mutations from atovaquone-resistant *P. jirovecii* into the cytochrome *b* gene of *Saccharomyces cerevisiae* and thus obtained cytochrome bc_1 complexes resistant to inhibition by atovaquone. In these enzymes, the IC_{50} for atovaquone increases from 25 nM for the enzyme from wild-type yeast to >500 nM for some of the mutated enzymes. Modeling of the changes in cytochrome *b* structure and atovaquone binding with the mutated bc_1 complexes provides the first quantitative explanation for the molecular basis of atovaquone resistance.

Pneumocystis jirovecii[1] pneumonia is the most serious and prevalent AIDS-associated opportunistic infection, and it is also the causative agent of *P. jirovecii* pneumonia in other immunocompromised patients, such as those undergoing therapy for cancer and organ transplantation. The intrapulmonary forms of this airborne fungal organism multiply extracellularly and fill the lung alveoli, leading to reduced gas exchange and blood oxygenation (1).

Atovaquone, a substituted hydroxynaphthoquinone (2, 3) was first used therapeutically as an anti-protozoal compound that has broad spectrum activity against apicomplexan parasites (4–6) and later was also shown to prevent and clear *P. jirovecii* pneumonia (7, 8). Atovaquone is now widely used as an important "second-line" therapy for prophylaxis and treatment of moderate cases of *Pneumocystis* infections (9, 10).

In recent years, spontaneously arising mutations that confer atovaquone resistance have resulted in the failure of atovaquone treatment and mortality of patients with *P. jirovecii* pneumonia. Consequently, a multi-center study was conducted to determine the reasons for the failure of this therapeutic agent (11, 12). Atovaquone has been shown to be a potent and specific inhibitor of the cytochrome bc_1 complex (13, 14), an essential respiratory enzyme present in the inner mitochondrial membrane. It appeared that mutations in the cytochrome *b* subunit of the cytochrome bc_1 complex of *P. jirovecii* were the cause of resistance to the drug. The relatively high frequency of spontaneously arising mutations that confer atovaquone resistance may be because the cytochrome *b* gene is located in the mitochondria where mutation rates are usually higher than in the nucleus due to the multi-copy nature of the mitochondrial genome.

The similarities of *P. jirovecii* to ascomycete fungi and the lack of an *in vitro* culture system for *P. jirovecii* suggest that *Saccharomyces cerevisiae* may be a useful organism in which to model the molecular basis of atovaquone resistance in *P. jirovecii* (15–18). There is a high degree of sequence identity in the regions of cytochrome *b* involved in atovaquone binding in the two fungal species, and the yeast is amenable to transformation of the mitochondrial genome (19–21). In addition, the cytochrome bc_1 complex of *S. cerevisiae* can be purified and its crystal structure is available (22). Thus, we characterized the interaction of atovaquone with the yeast bc_1 complex and developed a model of atovaquone binding to the ubiquinol oxidation pocket that accounts for the effects of this competitive inhibitor on the isolated enzyme (14).

We also recently developed a *S. cerevisiae* strain that is sensitive to atovaquone by deleting the genes for plasma membrane transporters that are otherwise responsible for efflux of the drug (23). Cytochrome *b* mutations associated with atovaquone resistance in *P. jirovecii* were then transferred into the atovaquone-sensitive *S. cerevisiae* by transformation of the mitochondrial genome. The resulting mutated yeast strains were atovaquone-resistant, and the cytochrome *c* reductase activities of the mitochondrial membranes exhibited significantly reduced sensitivity toward the drug (23). In this study, we have isolated the cytochrome bc_1 complexes from atovaquone-resistant yeast mutants and characterized the kinetic properties of the mutated enzymes and the interaction of the enzymes with atovaquone. We have also modeled the structural changes associated with the mutations *in silico* to describe the molecular basis of atovaquone resistance.

EXPERIMENTAL PROCEDURES

Materials—Yeast extract and peptone were from Difco. Nitrogen base without amino acids but with ammonium sulfate was from U. S.

* This work was supported by National Institutes of Health Research Grants GM 20379 (to B. L. T.) and AI46966 (to S. R. M.), a Medical Research Fellowship (to B. M.), and a Biotechnology and Biological Sciences Research Council Studentship (to P. H.). The costs of publication of this article were defrayed in part by the payment of page charges. This article must therefore be hereby marked "*advertisement*" in accordance with 18 U.S.C. Section 1734 solely to indicate this fact.

‖ To whom correspondence should be addressed: Dept. of Biochemistry, Dartmouth Medical School, 7200 Vail, Hanover, NH 03755. Tel.: 603-650-1621; E-mail: Trumpower@Dartmouth.edu.

[1] *P. jirovecii* was previously named *Pneumocystis carinii*.

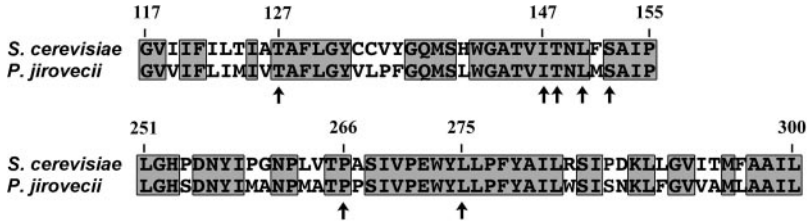

FIG. 1. **Sequence alignment of the cytochrome *b*s of *S. cerevisiae* and *P. jirovecii* in the highly conserved regions between amino acid residues 117–155 and 251–300.** The alignment was constructed using ClustalW and numbering from the yeast cytochrome *b*. The *arrows* show the positions of the mutated residues.

Biological. Dodecylmaltoside was obtained from Roche Applied Science. DEAE-Biogel A was obtained from Bio-Rad. Diisopropylfluorophosphate, decyl ubiquinone, and dithionite were purchased from Sigma. Stigmatellin was purchased from Fluka Biochemica. Atovaquone was a gift from GlaxoSmithKline.

Purification of and Assay of Cytochrome bc_1 Complexes—The cytochrome *b* mutations were introduced into the mitochondrial cytochrome *b* gene by biolistic transformation as described elsewhere (23). Wild-type and mutated yeast strains were grown in yeast extract/peptone/dextrose medium and harvested by centrifugation. Cytochrome bc_1 complexes were then isolated from the yeast mitochondrial membranes as described previously (24, 25) and concentrated by centrifugal filtration using Amicon® Centriprep YM-30 filtration tubes. Ubiquinol-cytochrome *c* reductase activities of the purified cytochrome bc_1 complexes were measured as described previously (14).

Western Blot Analysis of Cytochrome bc_1 Complexes—The Western blot analysis was performed using 2 pmol of purified cytochrome bc_1 complexes from wild-type and mutated strains. The proteins were resolved in a 15% SDS-PAGE gel and transferred to a nitrocellulose membrane using a Bio-Rad Mini-PROTEAN® II apparatus. The membranes were probed for iron-sulfur protein and cytochrome c_1 using monoclonal antibodies to the yeast proteins (26). The relative amounts of iron-sulfur protein and cytochrome c_1 were determined by scanning the Western blot and densitometry quantification using the NIH Image software (rsb.info.nih.gov/nih-image/).

Molecular Modeling—Molecular modeling was carried out on a Silicon Graphics O_2 work station using the commercially available Insight II® software package (Acclerys Inc., San Diego). The starting structure was the dimeric cytochrome bc_1 complex from *S. cerevisiae* as determined by x-ray crystallography to a resolution of 2.3 Å (Protein Data Bank code 1EZV) (22). Modeling was focused on two subunits, cytochrome *b* and the Rieske iron-sulfur protein, along with buried water molecules. The six *P. jirovecii* cytochrome *b* mutations that conferred atovaquone resistance in yeast were built into the previously modeled atovaquone-bound center P site (14) using the Biopolymer® module. Prior to molecular dynamics and energy minimization, the manual rotamer function was used to select the most plausible starting conformation for each residue. All of the modeling was done using the CFF91 force-field and a central flexible subset of amino acid residues surrounded by a 9.5-Å shell of fixed residues including atovaquone. The most distant residues were excluded from calculation in the interest of speed.

The mutations were divided into three modeling groups based on their proximity to atovaquone. The I147V, L150F, and L275F mutations were grouped together because of their direct interaction with atovaquone in the center P binding site. The flexible subsets for mutations L150F and L275F were defined by a 2.0-Å radius from the mutated residue to allow the pocket to accommodate the larger side chains. The flexible subset for mutation I147V consisted only of the mutated residue, because the mutation decreased the volume of the side chain. This minimal flexibility allowed evaluation of the energy cost that each mutation has on atovaquone binding. Using the same procedure as was used for the modeling of atovaquone into the wild-type structure (14), four simulated annealing runs were carried out on each mutant structure.

The T148I and S152A mutations were grouped together because of their locations in the cd1 helix facing away from the atovaquone binding pocket. The size of the flexible subsets was too great for effective simulated annealing modeling, so both mutations were modeled by molecular dynamics to equilibrium. The flexible subset consisted of the cd1 helix and its flanking loop regions. In the T148I model, a restraint was set up between Ser-152 and Lys-288 of cytochrome *b* to simulate the hydrogen bond connecting the ends of the cd1 and F1 helices. No restraint was used in the S152A model, because the mutation itself disrupted the hydrogen bond. The simulation temperature was kept constant at 800 K. Each simulation began with 5000 fentoseconds of equilibration using a 1.0-fentoseconds/iteration time step and the velocity scaling temperature control method. Molecular dynamics simulation was continued for an additional 50 picoseconds using a 0.5-fentoseconds/iteration time step and the more accurate Nosé temperature control method. Successful equilibration was judged by plotting both the running and batch averages for the total energy *versus* time. Equilibrium was reached when the batch-average energies oscillated smoothly around the constant running-average energy. Upon reaching equilibrium, the lowest energy structure from each run was selected for a full minimization using the same procedure as for the modeling of atovaquone in the wild-type structure.

The P266L mutation was modeled individually because of its unique location in the ef loop outside the inner shell of residues that coordinate the bound atovaquone. In the first set of runs, the flexible subset consisted of ef loop residues 264–272, nearby Met-139, and adjacent water molecules. This subset was chosen to allow any changes in backbone and side-chain conformations in the P266L mutant to propagate into the atovaquone binding pocket. In contrast to the other five mutant models, atovaquone and the iron-sulfur protein were excluded from simulation. This was done to model the position of the ef loop of cytochrome *b* before the binding of atovaquone, at which point the iron-sulfur protein has moved away from the binding pocket into its c_1 position. Several annealed dynamics runs were carried out on the unliganded P266L mutant structure and an unliganded wild-type control structure. The minimized results indicated that the P266L mutant endowed the ef loop with greater flexibility, allowing Ile-269 to move down into the binding pocket. Atovaquone and the iron-sulfur protein were reintroduced into the P266L and wild-type control models. In the final set of annealed dynamics runs, atovaquone and the iron-sulfur protein were fixed just as they were for the other five mutations. The flexible subset was focused to include only those residues from the first runs that came into direct contact with atovaquone.

To estimate the energy cost of binding atovaquone, we calculated the energy of each mutant structure with atovaquone bound and compared that to the energy of the wild-type enzyme with atovaquone bound. The structure of the atovaquone binding pocket in each of the atovaquone-resistant mutant models was optimized using a unique subset of flexible residues based on the location and nature of the mutation. In contrast, to facilitate comparison of changes in binding energy, the energy calculation used a common subset that included atovaquone, the residue His-181 from the iron-sulfur protein, cytochrome *b* residues within 4.0 Å of the inhibitor, and cytochrome *b* residues within 4.0 Å of the residue Glu-272 of cytochrome *b*. This calculated energy contained non-bonding interactions (van der Waals and electrostatic) and internal conformational energies of atovaquone and adjacent pocket residues.

RESULTS

Location of Cytochrome b Mutations in the Center P Ubiquinol Oxidation Pocket—The overall sequence identity of the cytochrome *b* subunits of the *S. cerevisiae* and *P. jirovecii* cytochrome bc_1 complexes is ~60%. In the regions of cytochrome *b* between amino acid residues 117–155 and 251–300 corresponding to the segments of the protein around the ubiquinol oxidation pocket where the resistance mutations occur in the *P. jirovecii* protein, the two cytochrome *b* sequences are 73% identical as shown in Fig. 1.

The structure of the ubiquinol oxidation site at center P with atovaquone bound with the location of the amino acid resides that are affected in the atovaquone-resistant cytochrome *b* mutants is shown in Fig. 2. In this modeled structure, the

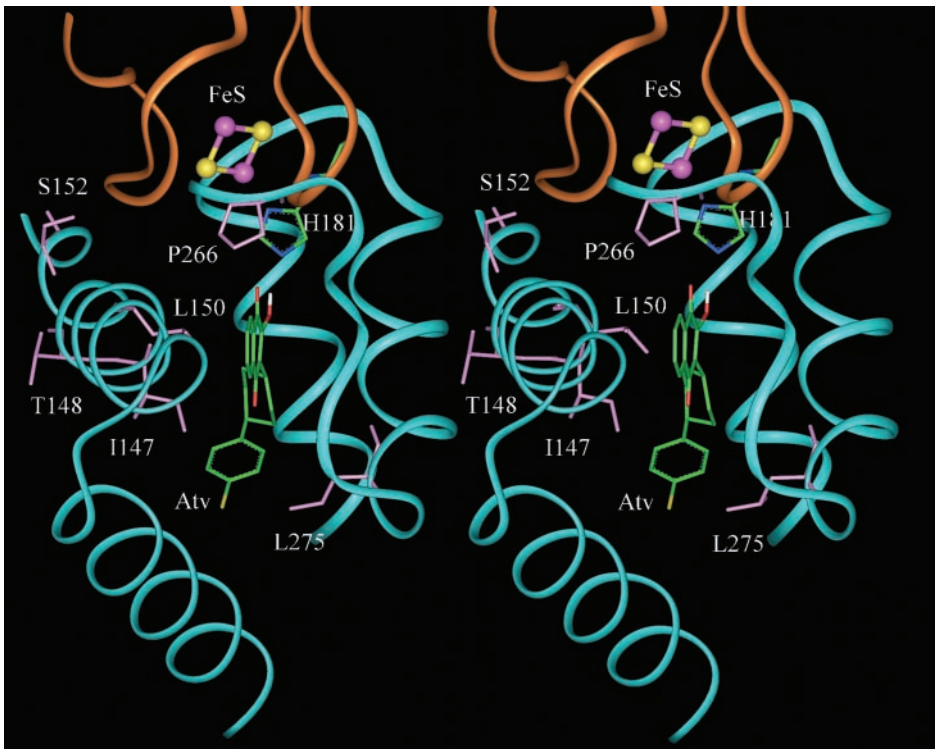

FIG. 2. **Stereoview of the atovaquone binding pocket of the yeast cytochrome bc_1 complex showing the location of mutations conferring resistance to atovaquone in *P. jirovecii*.** A portion of cytochrome *b* including the cd1 and ef helices, the ef loop, and part of helix C is shown in *cyan*, and a portion of the Rieske iron-sulfur protein including the loops that coordinate the iron-sulfur cluster is shown in *gold*. The iron-sulfur cluster is at the *top* with iron and sulfur atoms *colored purple* and *yellow*, respectively. The hydroxynaphthoquinone ring of atovaquone points toward the front, and the chlorophenyl ring extends to the rear. The carbon atoms in atovaquone and His-181 of the Rieske protein are *colored green*, oxygen atoms are *red*, nitrogen atoms are *blue*, and hydrogen atoms are *white*. The cytochrome *b* residues that are changed in the atovaquone-resistant yeast mutants are *colored purple*.

hydroxyl group of the hydroxynaphthoquinone binds via a hydrogen bond to a imidazole nitrogen of His-181 of the Rieske protein (14). On the opposite side of the ring system, the carbonyl group at position 4 on the quinone ring interacts via a water molecule with Glu-272 of cytochrome *b*. This structure accounts for the effects of atovaquone on the Rieske iron-sulfur protein and is also consistent with the crystal structure of the yeast bc_1 complex with another hydroxyquinone bound in the center P pocket (27).

As described below, the six *P. jirovecii* cytochrome *b* mutations showing atovaquone resistance were built into this previously modeled ubiquinol oxidation site at center P to analyze the structural changes resulting from the mutations. These six mutations are I147V, T148I, L150F, S152A, P266L, and L275F. Three of the amino acid residues (Ile-147, Leu-150, and Leu-275) that are mutated in the *P. jirovecii* cytochrome *b* interact directly with atovaquone in the modeled structure as shown in Fig. 2. Two of the affected residues, Ser-152 and Thr-148, are in the cd1 helix facing away from the atovaquone binding pocket. One residue, Pro-266, is in the ef loop outside the inner shell of residues that coordinates the bound atovaquone.

Effect of Cytochrome b Mutations on Activities of the Cytochrome bc_1 Complexes—We introduced seven mutations that have been linked to atovaquone resistance in P. jirovecii into the yeast cytochrome *b* gene (23). Ubiquinol-cytochrome *c* reductase activities were measured in both mitochondrial membranes and the purified enzymes from each mutant and are summarized in Table I and Fig. 3. The activities of the bc_1 complexes from most of the mutated strains increased by varying amounts relative to that in the membranes during purification of the enzymes. A similar increase during purification is seen with the enzyme from wild-type yeast and from bovine heart mitochondria (25). These increases in activity occur when the enzyme is dispersed from the membrane with detergent, which presumably results in better substrate accessibility to the enzyme. For this reason, we feel that measurements of activity and related kinetic parameters are more reliably represented with the purified enzymes.

TABLE I
Kinetic parameters of cytochrome bc_1 complexes from atovaquone-resistant yeast mutants

ND, not determined.

Yeast strains	k_{cat}	K_m	V_m
	s^{-1}	μM	s^{-1}
Wild type	220	13	270
T127I	15	ND	ND
I147V	120	8	160
T148I	200	13	200
L150F	30	ND	ND
S152A	30	ND	ND
P266L	70	9	85
L275F	200	13	280

The exception to the increased activity during purification was in our attempt to purify the bc_1 complex from the T127I mutant strain in which case there was a 60% decrease in activity of the purified bc_1 complex compared with the enzyme in the membranes (Table I and Fig. 3). Loss of iron-sulfur protein and/or damage to cytochrome *b* is the most common form of damage to the cytochrome bc_1 complex during purification. Thus, we thus analyzed the purified enzymes by Western blots and optical absorption spectroscopy of the bc_1 complexes from these strains. The Western blots (Fig. 4) and absorption spectra (data not shown) revealed that, with the exception of T127I, the mutations and the purification procedures neither affected the iron-sulfur protein subunit stoichiometry nor the heme composition of the bc_1 complexes. The Western blots showed that the loss of activity during purification of the bc_1 complex from the T127I mutant could be attributed to loss of iron-sulfur protein (Fig. 4). Because of the extensive loss of activity during purification of this bc_1 complex and because the T127I mutant did not exhibit resistance to atovaquone (23), the enzyme from this mutant was not further characterized.

Effect of Cytochrome b Mutations on Inhibition of the bc_1 Complex by Atovaquone—Ubiquinol-cytochrome c reductase activities of the bc_1 complexes from the wild-type and atova-

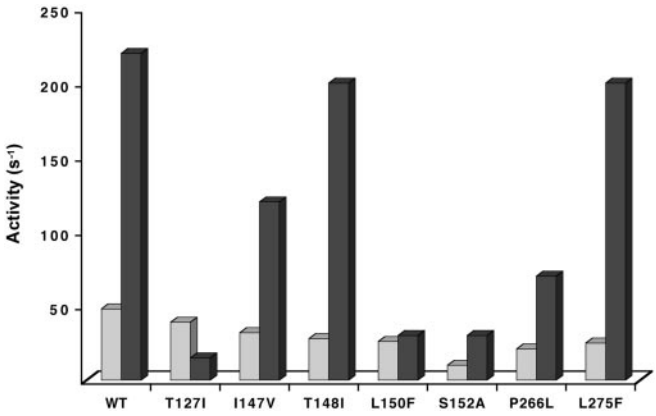

FIG. 3. **Ubiquinol-cytochrome *c* reductase activities of mitochondrial membranes and purified cytochrome bc_1 complexes from atovaquone-resistant mutants.** Activities of the membranes (*light gray*) and purified bc_1 complexes (*black*) are expressed as moles of cytochrome *c* reduced per mole of enzyme per second.

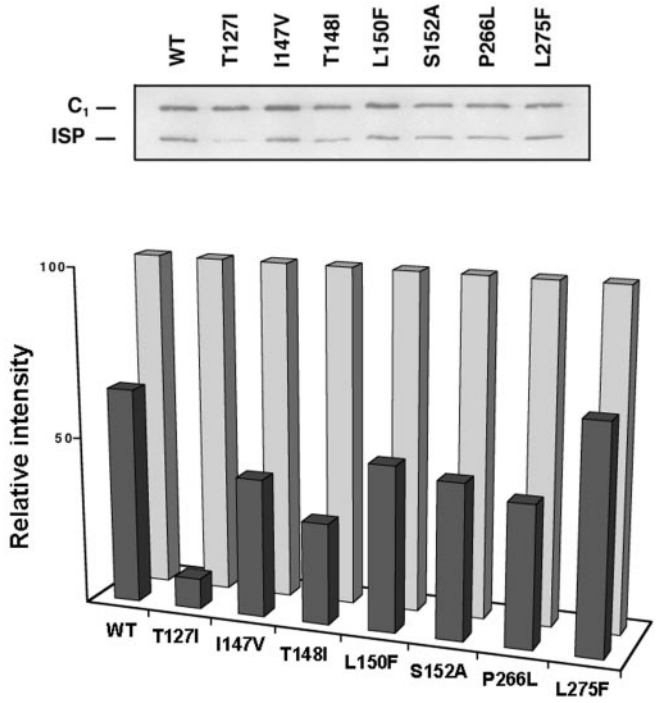

FIG. 4. **Immunoblot analysis of cytochrome bc_1 complexes with cytochrome *b* mutations.** Cytochrome bc_1 complexes were resolved by SDS-PAGE, and the Western blot was probed with monoclonal antibodies against yeast iron-sulfur protein and cytochrome c_1. The Western blot is shown at the *top*, and the relative amounts of iron-sulfur protein compared with cytochrome c_1 determined by densitometry scanning of the Western blot are shown at the *bottom*. The relative amounts of cytochrome c_1 were arbitrarily set to 100% to allow comparison of the samples.

quone-resistant yeast strains were measured in the presence of increasing concentrations of atovaquone to test whether sensitivity of the enzymes to the bc_1 inhibitor was altered by the cytochrome *b* mutations. Similar measurements were made with stigmatellin, another inhibitor that binds to the ubiquinol oxidation pocket at center P.

We previously showed that atovaquone is a competitive inhibitor of the bc_1 complex (14), and as shown in Fig. 5, it inhibits the activity of the bc_1 complex from wild-type yeast with an IC_{50} of ~25 nM. The cytochrome *b* mutations that confer atovaquone resistance to the yeast mutants alter the IC_{50} for inhibition of the bc_1 complex by varying amounts. The T148I mutation has the smallest effect, and it increases the IC_{50} ~2-fold to 60 nM. Interestingly, this mutation seems to impact on the yeast bc_1 complex assembly because it caused a 30% decrease in cytochrome *b* content as estimated from optical spectra of whole cells (23). The I147V, L150F, and P266L mutations increase the IC_{50} for inhibition of the bc_1 complex to 150–300 nM. The L275F and S152A mutations increase the IC_{50} to 500–800 nM. This result corresponds to a 20-fold increase over that of the wild-type enzyme.

The cytochrome *b* mutations had little or no effect on inhibition of the enzyme by stigmatellin. Interestingly, the T148I mutation, which had the smallest effect on inhibition of the enzyme by atovaquone, caused the largest change in IC_{50} for inhibition by stigmatellin. This lack of cross-resistance is discussed in more detail below.

Because atovaquone is a competitive inhibitor of the bc_1 complex, we also examined how the resistance mutations affected the interaction of the substrate with the enzyme. As can be seen in Table I, two of the mutations, T148I and L275F, had no significant effect on activity or K_m for ubiquinol oxidation. There was a modest decrease in K_m for ubiquinol oxidation in enzymes from two of the resistant mutants, I147V and P266L, and there was also a significant drop in activity of the enzymes from these two mutants. The L150F and S152A mutations caused the ubiquinol-cytochrome *c* reductase activities of the isolated bc_1 complexes to drop to 5–10% of the activity of the enzyme from wild-type yeast. These activities were too low to permit accurate evaluation of the kinetic parameters for ubiquinol oxidation by the purified enzymes from these strains.

Molecular Modeling of Structural Changes in Cytochrome b Caused by Mutations Conferring Resistance to Atovaquone—The six *P. jirovecii* cytochrome *b* mutations showing atovaquone resistance were built into the previously modeled atovaquone-bound center P site (14), and the structural changes resulting from the mutations were modeled *in silico*. The mutations were divided into three groups based on their proximity to atovaquone. The I147V, L275F, and L150F mutations shown in Fig. 6, *panels A–C*, were grouped together because of their direct interaction with atovaquone in the center P binding site. The modeling of the L275F (Fig. 6*B*) and L150F (Fig. 6*C*) mutations indicates that they increase the steric volume in the atovaquone binding pocket, which would interfere with binding of the inhibitor. Interestingly, the I147V (Fig. 6*A*) mutation decreases van der Waals and electrostatic interactions between the atovaquone and residues in the binding pocket, which would increase the binding energy.

The T148I and S152A mutations shown in Fig. 7, *A* and *B*, were grouped together because of their locations in the cd1 helix facing away from the atovaquone binding pocket. In these mutants, the resistance appeared to be attributed to loss of a hydrogen bond between a residue positioned on the side of the cd1 helix (Ser-152 or Thr-148) and an anchor residue (Lys-288 on helix F1 or Trp-166 on helix cd2). These disruptions caused significant changes in the structure and stability of the cd1 helix. Consequently, the hydrophobic residues facing the binding pocket, especially Val-146 and Ile-147 on the cd1 helix, displayed a change from their original positions resulting in a reduction of the affinity of the inhibitor. This effect was more important in the S152A mutation than in the T148I mutation, both in terms of resistance and activity.

The P266L mutation shown in Fig. 6*D* was modeled individually because of its unique location in the ef loop, outside the inner shell of residues that coordinate the bound atovaquone. The resulting model revealed that the P266L mutation caused a significant change in the geometry of the ef loop. Consequently, Ile-269 moved into the atovaquone binding pocket, which would cause a reduction in binding affinity.

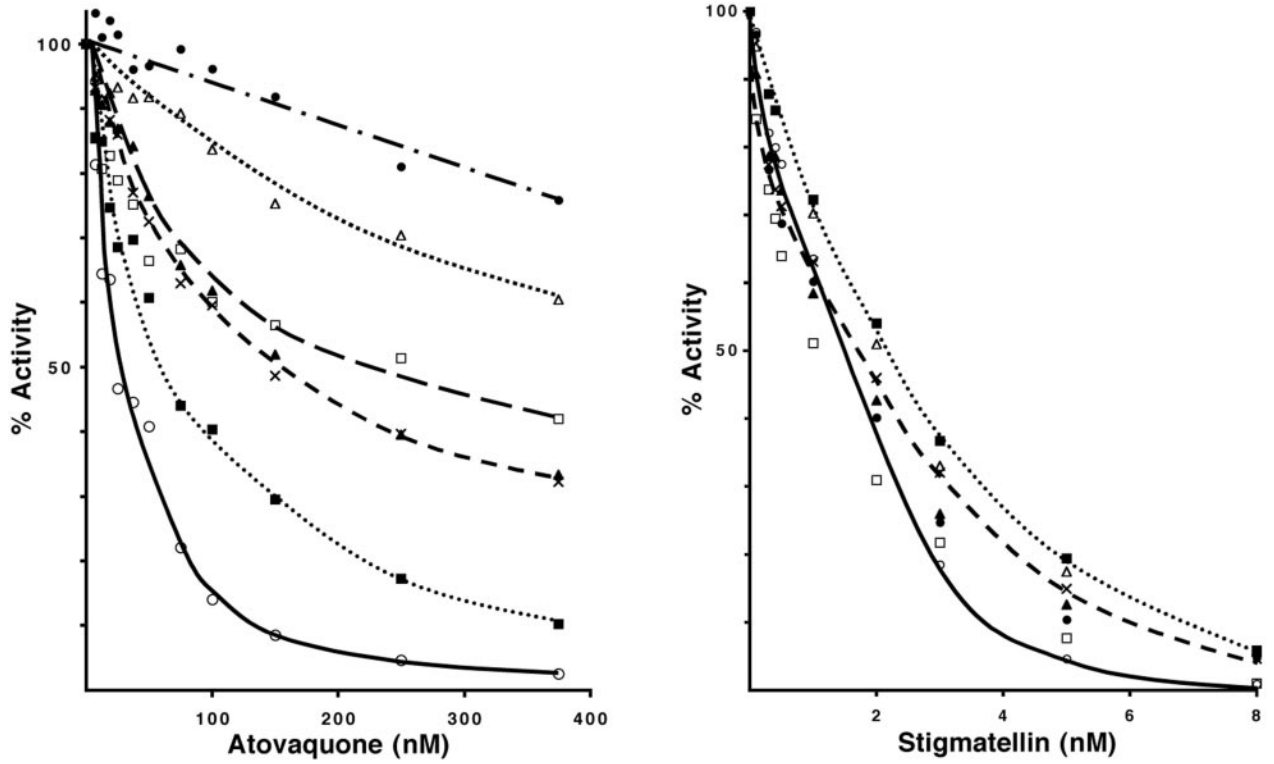

FIG. 5. **Efficacy of inhibition of wild-type and mutated bc_1 complexes by atovaquone and stigmatellin.** Ubiquinol-cytochrome *c* reductase activities of purified bc_1 complexes were measured in the presence of increasing concentrations of atovaquone or stigmatellin. Activities are expressed as a percentage of the activity of each bc_1 complex in the absence of inhibitor, which are listed in Table I. The *left panel* shows inhibition of the enzymes by atovaquone, and the *right panel* shows inhibition by stigmatellin. Activities for the enzymes from the various yeast are indicated as follows: wild type (*open circles*); T148I (*solid squares*); I147V (*crosses*); L150F (*solid triangles*); P266L (*open squares*); L275F (*open triangles*); and S152A (*solid circles*).

Calculation of Changes in Atovaquone Binding Energy Resulting from Mutations in Cytochrome b—To test how well the molecular modeling predicted the structural changes in the atovaquone binding pocket, we calculated the energy required for binding atovaquone with each of the modeled structures. We then compared the calculated changes in binding energy with the experimentally measured changes in IC_{50} values. The changes in atovaquone binding energy with the bc_1 complexes from the mutants relative to the binding energy obtained for the wild-type enzyme and the change in IC_{50} values for the mutant enzymes compared with the wild-type enzyme are shown in Fig. 8. The relative increase in calculated binding energy correlates well with the relative increase in IC_{50} for the bc_1 complex from each of the mutants, with the exception of the S152A mutant. This mutation caused the largest change in IC_{50}, but the calculated increase in binding energy was not the largest. This discrepancy can be attributed to the fact that the S152A mutation is distal to the atovaquone binding pocket, and there is thus more uncertainly associated with the molecular modeling of the structural change associated with this mutation.

DISCUSSION

We have used the yeast cytochrome bc_1 complex as a surrogate to understand the molecular basis of atovaquone interaction with the analogous enzyme of *P. jirovecii*, a fungal pathogen. The yeast enzyme is amenable to modification by site-directed mutagenesis, a high resolution crystal structure of the yeast enzyme is available (22), and the enzyme can be isolated for biochemical and biophysical characterization. We have thus elucidated the mechanism of atovaquone inhibition of the yeast bc_1 complex and developed a molecular model of atovaquone interaction that accounts for the effects of the inhibitor on the isolated enzyme and also accounts for the differential efficacy of inhibition of the fungal *versus* mammalian enzymes (14). The interaction of atovaquone with the yeast bc_1 complex is very similar to the interaction of another hydroxyquinone inhibitor with the enzyme for which a crystal structure is available (27)

Notably, the hydroxyl group of the hydroxynaphthoquinone binds via a hydrogen bond to the nitrogen of His-181 of the Rieske protein. On the opposite side of the ring system, the carbonyl group at position 4 of the quinone ring of atovaquone interacts via a water molecule with Glu-272 of cytochrome *b*. The rest of the molecular interaction is essentially hydrophobic with a network of aromatic and aliphatic side chains surrounding the inhibitor and constituted by the regions 117–155 and 251–300 of the yeast cytochrome *b*.

In this study, we have characterized cytochrome bc_1 complexes with mutations in cytochrome *b* that confer resistance to atovaquone in yeast and in *P. jirovecii*. All of the mutations were localized around the ubiquinol binding site (Fig. 2). Some of the affected amino acids extend directly into the atovaquone binding pocket, whereas others affect the pocket indirectly. One of the mutant alleles, L275F, is naturally occurring in mammals and is primarily responsible for the differential efficacy of the therapeutic in the fungus *versus* the mammalian host (14). Thus, this is an interesting example of a pathogen acquiring protective resistance by mimicking its human host.

In the cases where the mutated residues interacted directly with atovaquone (I147V, L150F, and L275F), the molecular modeling strategies were straightforward, focusing only on the region in close proximity to the binding site. The leucine to phenylalanine substitutions (L150F and L275F) created an increase in steric volume in the atovaquone binding pocket, which reduces the affinity for the inhibitor. Interestingly, in

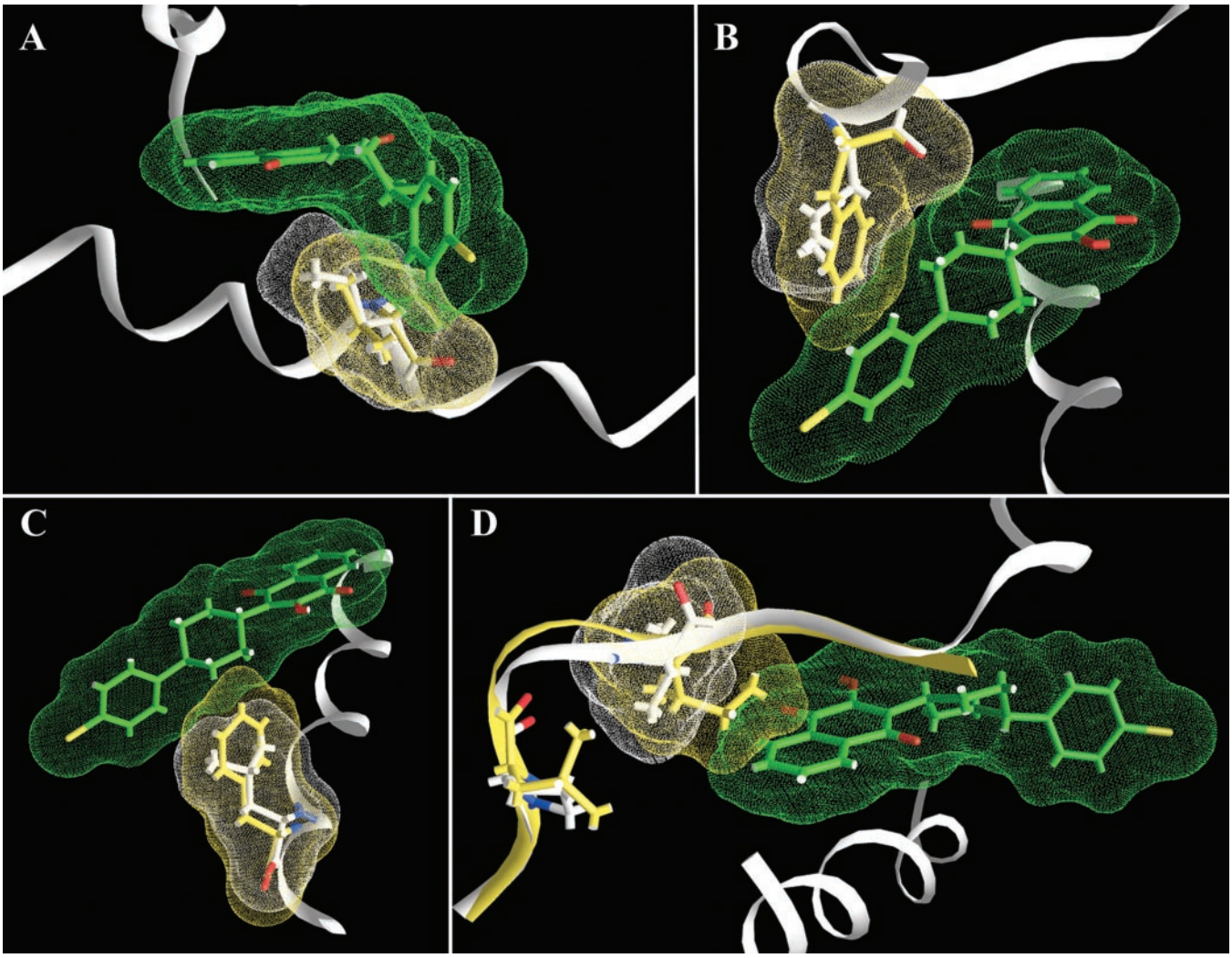

FIG. 6. **Molecular modeling of atovaquone-resistant mutations from *P. jirovecii* that are in the atovaquone-binding Qp pocket in *S. cerevisiae*.** Atovaquone (in *green* with oxygen atoms *red* and hydrogen atoms *white*), the wild-type residues (in *white*) and mutated residues (in *yellow*) are shown along with the cd1 helix and ef loop (both in *light gray*) to provide a relative perspective for the four panels. Van der Waals radii are represented by *dots*. The mutations depicted are I147V (*panel A*), L275F (*panel B*), L150F (*panel C*), and P266L (*panel D*).

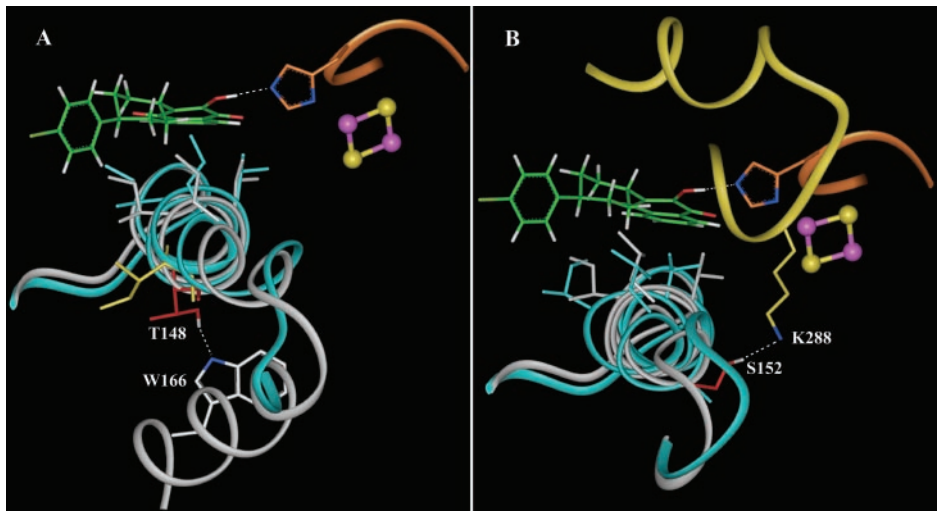

FIG. 7. **Molecular modeling of atovaquone-resistant mutations from *P. jirovecii* that are distal to the atovaquone-binding Qp pocket in *S. cerevisiae*.** Atovaquone (in *green* with oxygen atoms *red* and hydrogen atoms *white*), a portion of the Rieske iron-sulfur protein (in *gold* with iron and sulfur atoms *colored purple* and *yellow*, respectively), the cd1 helix in the wild-type cytochrome *b* (in *light gray*), and the cd1 helix in the mutated cytochrome *b* (in *cyan*) are shown. Thr-148, Ser-152, Trp-166, and Lys-288 are labeled, and hydrogen bonds are represented by *dashed lines*. Van der Waals radii are represented by *dots*. The mutations depicted are T148I (*panel A*) and S152A (*panel B*).

another mutation found near the binding site, I147V, the resistance is generated by a decrease of non-bonding interactions between atovaquone and the binding pocket when changing from isoleucine to valine. This was confirmed by a separate calculation of the contribution of the hydrophobic terms to the binding energy (data not shown). For these mutations that impacted directly on the atovaquone binding pocket, there was relatively good agreement between theoretically calculated changes in binding energy and the experimentally measured changes in IC_{50} values.

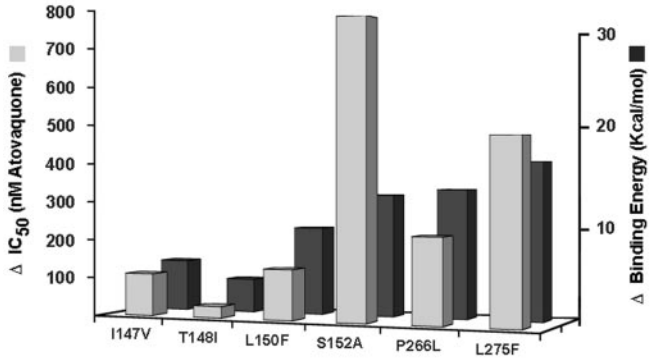

FIG. 8. **Measured changes in atovaquone inhibition and modeled changes in atovaquone binding with atovaquone-resistant cytochrome bc_1 complexes.** The *light gray bars* indicate the change in IC_{50} for inhibition of the bc_1 complexes by atovaquone compared with inhibition of the enzyme from wild-type yeast. The *dark bars* show the calculated change in binding energy for atovaquone with each of the mutated bc_1 complexes *versus* that with the wild-type enzyme.

For the distal mutations (T148I, S152A, and P266L), molecular modeling necessitated inclusion of a larger area around the binding site. Because Thr-148 and Ser-152 were both located on the side of the cd1 helix opposite the pocket, direct interactions could not account for changes in atovaquone affinity. In these cases, the resistance appeared to be generated by the loss of a hydrogen bond between a residue positioned on the side of the cd1 helix and an anchor residue on helix F1 or helix cd2. Molecular modeling showed that such disruptions caused significant changes in the structure and stability of the cd1 helix. Consequently, hydrophobic residues on the cd1 helix facing the binding pocket and interacting with the atovaquone changed position, resulting in a reduction of the affinity of the inhibitor. For the S152A mutation, the calculated change in binding energy was significantly less than the measured change in IC_{50} value. This difference suggests that this mutation caused an even greater change in the binding pocket than was predicted by the molecular modeling.

The P266L mutation necessitated a different setup for computer modeling because of the distance between this residue and the atovaquone. Pro-266 is located in the ef loop, which is part of the iron-sulfur protein-docking crevice. Mutations on this segment of the cytochrome *b* have been reported to interfere with docking of the iron-sulfur protein (28). To be able to simulate a change in the configuration in this area, the iron-sulfur protein was removed from the model to allow the ef loop to move freely. This setting simulated the bc_1 complex with the iron-sulfur protein in the distal position. The resulting computerized model revealed that the P266L mutation caused a significant change in the geometry of the ef loop. Consequently, the mutant Leu-266 residue induced a shift in residue Ile-269 toward the atovaquone binding pocket, causing a reduction in binding affinity. For this mutant also, the calculated change in binding energy increased by approximately the same amount as the measured change in IC_{50}.

Most of the cytochrome *b* mutations that increased the IC_{50} values for atovaquone inhibition of the bc_1 complex did not noticeably effect the inhibition by stigmatellin. However, because the K_i for stigmatellin with the yeast bc_1 complex is approximately equal to the concentration of enzyme in the cytochrome *c* reductase assay (29), small changes in binding affinity would go undetected. The lack of cross-resistance to atovaquone and stigmatellin indicates that the amino acid residues that determine efficacy of binding are different for the two ligands. Much of the stigmatellin binding energy appears to derive from interaction of its long substituted alkenyl side chain with cytochrome *b* (22), which agrees with the finding that slight alterations in this part of the ligand significantly decrease the binding affinity (30). Most of the atovaquone mutations studied here impacted specifically the binding of the naphthoquinone ring system to the active site and are located far from the cytochrome *b* pocket where the stigmatellin side chain interacts (22). Thus, it is not surprising that more extensive cross-inhibition between the two inhibitors was not observed. The I147V and T148I mutations, which had the least effect on atovaquone inhibition, had the largest effect on stigmatellin inhibition. Other mutations at positions 147 and 148 have been previously reported as conferring stigmatellin resistance in yeast (31) and in mouse (32).

It is interesting to observe that multiple mutations around the binding site can all lead to atovaquone resistance while preserving a functional bc_1 complex. With the exception of one case (I147V) in which a loss in non-bonding interactions was observed, all of the other mutations used directly or indirectly the same mechanism to decrease the affinity for the drug by reducing the volume of the binding pocket. There are probably many other potential positions in the segment of cytochrome *b* between residues 117–155 and 255–300 that could confer atovaquone resistance through a similar mechanism. This may substantially increase the probability of the appearance of mutations that confer atovaquone resistance and may explain why they emerged so rapidly when the drug was used only as a monotherapy to prevent and cure *P. falciparum* (33). In this organism also, the mutations conferring resistance surround the atovaquone binding pocket including M139I and G291D (34), L282F (35), and Y279C (36). In an attempt to overcome this problem, atovaquone is now used in a synergic combination with proguanil hydrochloride (Malarone®, GlaxoSmith-Kline) in the treatment of malaria (36).

REFERENCES

1. Cushion, M. T. (1994) in *Lung Biology in Health and Disease* (Walzer, P. D., ed) Vol. 69, pp. 123–140, Marcel Dekker, Inc., New York
2. Wendel, W. B. (1946) *Fed. Proc.* **5,** 406–407
3. Hudson, T., Dickins, M., Ginger, C. D., Gutteridge, W. E., Holdich, T., Hutchinson, D. B. A., Pudney, M., Randall, A. W., and Latter, V. S. (1991) *Drugs Exp. Clin. Res.* **17,** 427–435
4. Gutteridge, W. E. (1989) *J. R. Soc. Med.* **82,** Suppl. 17, 63–66
5. Araujo, F. G., Huskinson, J., and Remington, J. S. (1991) *Antimicrob. Agents Chemother.* **35,** 293–299
6. Hughes, W. T., and Oz, H. S. (1995) *J. Infect. Dis.* **172,** 1042–1046
7. Hughes, W. T., Gray, V. L., Gutteridge, W. E., Latter, V. S., and Pudney, M. (1990) *Antimicrob. Agents Chemother.* **34,** 225–228
8. Gutteridge, W. E. (1991) *J. Protozool.* **38,** 141S-143S
9. Chan, C., Montaner, J., Lefebvre, E. A., Morey G., Dohn, M., McIvor, R. A., Scott, J., Marina R., and Caldwell P. (1999) *J. Infect. Dis.* **180,** 369–376
10. El-Sadr, W. M., Murphy, R. L., Yurik, T. M., Luskin-Hawk, R., Cheung, T. W., Balfour, H. H., Jr., Eng, R., Hooton, T. M., Kerkering, T. M., Schutz, M., van der Horst, C., and Hafner R. (1998) *N. Engl. J. Med.* **339,** 1889–1895
11. Walker, D., Wakefield, A., Dohn, M., Miller, R., Baughman, R., Hossler, P., Bartlett, M., Smith, J., Kazanjian, P., and Meshnick S. R. (1998) *J. Infect. Dis.* **178,** 1767–1775
12. Kazanjian, P., Armstrong, W., Hossler, P. A., Huang, L., Beard, C. B., Carter, J., Crane, L., Duchin, J., Burman, W., Richardson, J., and Meshnick S. R. (2001) *J. Infect. Dis.* **183,** 819–822
13. Fry, M., and Pudney, M. (1992) *Biochem. Pharmacol.* **43,** 1545–1553
14. Kessl, J., Lange B. B., Merbitz-Zahradnick, T., Zwicker, K., Hill, P., Meunier, B., Meshnick, S., and Trumpower, B. L. (2003) *J. Biol. Chem.* **278,** 31312–31318
15. Bruns, T. D., Vilgalys, R., Barns, S. M., Gonzalez, D., Hibbett, D. S., Lane, D. J., Simon, L., Stickel, S., Szaro, T. M., Weisburg, W. G., and Sogin, M. L. (1992) *Mol. Phylogenet. Evol.* **1,** 231–241
16. Ludewig, G., and Staben, C. (1994) *Antimicrob. Agents Chemother.* **38,** 2850–2856
17. Ludewig, G., Williams, J. M., Li, Y., and Staben, C. (1994) *Antimicrob. Agents Chemother.* **38,** 1123–1128
18. Hatfield, C., Kasarskis, A., and Staben, C. (1991) *J. Protozool.* **38,** S70–S71
19. Fox, T. D., Sanford, J. C., and McMullin, T. W. (1988) *Proc. Natl. Acad. Sci. U. S. A.* **85,** 7288–7292
20. Butow, R. A., Henke, R. M., Moran, J. V., Belcher, S. M., and Perlman, P. S. (1996) *Methods Enzymol.* **264,** 265–278
21. Bonnefoy, N., and Fox, T. D. (2001) *Methods Cell Biol.* **65,** 381–396
22. Hunte, C., Koepke, J., Lange, C., Roßmanith, T., and Mitchel, H. (2000) *Structure* **8,** 669–684
23. Hill, P., Kessl, J., Fisher, N., Meshnick, S., Trumpower, B. L., and Meunier B. (2003)) *Antimicrob. Agents Chemother.* **47,** 2725–2731

24. Snyder, C. H., and Trumpower, B. L. (1999) *J. Biol. Chem.* **274,** 31209–31216
25. Ljungdahl, P. O., Pennoyer, J. D., Robertson, D., and Trumpower, B. L. (1987) *Biochim. Biophys. Acta* **891,** 227–242
26. Ljungdahl, P. O., Beckmann, J. D., and Trumpower, B. L. (1989) *J. Biol. Chem.* **264,** 3723–3731
27. Palsdottir, H., Gomez Lojero, C., Trumpower, B. L., and Hunte, C., (2003) *J. Biol. Chem.* **278,** 31303–31311
28. Darrouzet, E., and Daldal, F. (2003) *Biochem.* **42,** 1499–1507
29. Gutierrez-Cirlos, E. B., and Trumpower, B. L. (2002) *J. Biol. Chem.* **277,** 1195–1202
30. Ohnishi, T., Brandt, U., and von Jagow, G (1988) *Eur. J. Biochem.* **176,** 385–389
31. di Rago, J.-P., Coppee, J.-Y., and Colson, A.-M. (1989) *J. Biol. Chem.* **264,** 14543–14548
32. Howell, N., and Gilbert, K. (1988) *J. Mol. Biol.* **203,** 607–618
33. Looareesuwan, S., Viravan, C., Webster, H. K., Kyle, D. E., Hutchinson, D. B., and Canfield, C. J. (1996) *Am. J. Trop. Med. Hyg.* **54,** 62–66
34. Korsinczky, M., Chen, N., Kotecka, B., Saul, A., Rieckmann, K., and Cheng, Q. (2000) *Antimicrob. Agents Chemother.* **44,** 2100–2108
35. Schwobel, B., Alifrangis, M., Salanti, A., and Jelinek, T. (2003) *Malaria J.* **2,** 5
36. Srivastava, I. K., and Vaidya, A. B. (1999) *Antimicrob. Agents Chemother.* **43,** 1334–1339